PERIODICA POLYTECHNICA SER. MECH. ENG. VOL. 36, NO. 1, PP. 61-84 (1992)

PERFORMANCE CHARACTERISTICS OF A CONSTANT FLOW VALVE COMPENSATED MULTIPLE HOLE-ENTRY HYBRID FLEXIBLE JOURNAL BEARINGS

S. C. SHARMA, S. C. JAIN, and R. SINHASAN

Department of Mechanical and Industrial Engg.
University of Roorkee

Received September 27, 1991.

Abstract

The multiple hole-entry flexible journal bearing configurations with constant flow valve compensation have been theoretically studied to determine the effects of bearing shell flexibility on the bearing performance characteristic. Finite element method has been used to obtain solutions of 3-dimensional elasticity equations and Reynolds equation. The non-dimensional parameter $\overline{C}_d$ is defined to account for the flexibility of bearing shell.

Bearing performance characteristics have been presented for wide range of representative values of deformation coefficient ($\overline{C}_d$) and non-dimensional external load ($\overline{W}_o$). The results indicate that the bearing performance characteristic are significantly affected by bearing shell flexibility, both for hydrostatic ($\Omega = 0.0$) and hybrid ($\Omega \neq 0.0$) modes of operations.

Keywords: flexible journal bearing, flow valve compensation, performance characteristics.

Nomenclature

a : Radius of capillary ,
a_b : Bearing land width in axial direction ,
c : Radial clearance ,
c_{ij} : Damping coefficient ($i, j = 1, 2$) ,
D : Journal diameter ,
e : Journal Eccentricity ,
E : Modulus of elasticity of Bearing material ,
F : Resultant fluid film reaction $\left[\frac{\partial h}{\partial t} \neq 0\right]$,
F_o : Resultant fluid film reaction $\left[\frac{\partial h}{\partial t} = 0\right]$,
F_{ox}, F_{oz} : x and z components of fluid film reaction $\left[\frac{\partial h}{\partial t} = 0\right]$,
g : Acceleration due to gravity ,
h : Fluid film thickness ,
h_{min} : Minimum fluid film thickness ,
M_c : Critical mass of journal ,
M_j : Journal mass Z ,

l : Capillary length ,
L : Journal Bearing length,
N : Rotational speed,
O_b : Bearing centre,
O_j : Journal centre,
p : Pressure,
p_c : Pocket pressure $\left[\frac{\partial h}{\partial t} \gtreqless 0\right]$,
p_s : Supply pressure,
Q : Total bearing flow,
Q_n : Flow through constant flow valve restrictor,
R_j : Radius of journal,
S_{ij} : Fluid film stiffness coefficient ($i, j = 1, \ldots, 2$),
t : time,
t_h : Thickness of bearing shell,
U : Surface speed ($= \omega_j R_j$),
u, v, w : Components of bearing shell deformation,
$\overline{W}_o$: External load,
X, Y, Z : Cartesian co-ordinate system,
X_j, Z_j : Journal centre co-ordinates,
μ : Dynamic viscosity of the lubricant,
ω_j : Journal rotational speed,
$\overline{\omega}_{th}$: Threshold speed,
$\overline{\omega}_d$: Damped frequency of whirl,
ω_l : $\left[\frac{g}{c}\right]^{1/2}$,
ρ : Density of the lubricant

Non-Dimensional Parameters for Journal Bearings

$$\overline{C}_{ij} = C_{ij}\left[\frac{c^3}{\mu \cdot R_j^4}\right],$$

$$\overline{C}_{s1} = \frac{3\pi a^4}{2 \cdot c^3 \cdot l} \qquad \text{for capillary restrictor},$$

$$\overline{C}_{s2} = \frac{\overline{C}_{s1}}{6},$$

$$\overline{C}_d = \left[\frac{P_s}{E}\right] \cdot \left[\frac{t_h}{c}\right],$$

$$\overline{F}, \overline{F}_o, \overline{F}_{ox}, \overline{F}_{oz}, \overline{W}_o = \frac{(\overline{F}, \overline{F}_o, \overline{F}_{ox}, \overline{F}_{oz}, \overline{W}_o)}{p_s} \cdot R_j^2,$$

$$\overline{h}\,,\overline{h}_{\min} = \frac{(h\,,h_{\min})}{c}\,,$$

$$(\overline{M}_{\mathrm{c}}\,,\overline{M}_{\mathrm{j}}) = (M_{\mathrm{c}}\,,M_{\mathrm{j}})\left[\frac{c^2\cdot p_{\mathrm{s}}}{\mu\cdot R_j^2\cdot\omega_{\mathrm{I}}}\right],$$

$$\dot{\overline{h}} = \frac{\partial\overline{h}}{\partial\overline{\tau}}\,,$$

$$\overline{p}\,,\overline{p}_{\max} = \frac{(p\,,p_{\max})}{p_{\mathrm{s}}}\,,$$

$$\overline{Q} = \left[\frac{\mu}{c^3\cdot p_{\mathrm{s}}}\right]\cdot Q\,,$$

$$\overline{S}_{ij} = \left[\frac{c}{p_{\mathrm{s}}\cdot R_j^2}\right]\cdot S_{ij}\,,$$

$$\overline{t}_h = \frac{t_h}{R_j}\,,$$

$$\overline{u}\,,\overline{v}\,,\overline{w} = \frac{(u\,,v\,,w)}{c}\,,$$

$$\overline{X}_j = \frac{X_j}{c}\,,$$

$$\overline{Z}_j = \frac{Z_j}{c}\,,$$

$\varepsilon = \dfrac{e}{c}$ eccentricity ratio,

$\alpha = \dfrac{X}{R_j}$ circumferential co-ordinate,

$\beta = \dfrac{X}{R_j}$ Axial co–ordinate,

$\phi =$ Attitude angle,

$\lambda = \dfrac{L}{D}$, Aspect ratio,

$\nu =$ Poisson's ratio,

$\Omega = \dfrac{\omega_{\mathrm{j}}}{\frac{c^2\cdot p_{\mathrm{s}}}{\mu\cdot R_j^2}}$ speed parameter,

$$\tau = \frac{t}{\frac{\mu\cdot R_j^2}{c^2 p_{\mathrm{s}}}}\,,$$

$$\overline{\omega}_{\mathrm{th}}\,,\overline{\omega}_{\mathrm{d}} = \frac{(\omega_{\mathrm{th}}\,,\omega_{\mathrm{d}})}{\omega_{\mathrm{I}}}\,.$$

Subscripts and Supercripts

b : bearing,
c : pocket,
j : journal,
o : static equilibrium or steady state position,
R : restrictor,
s : supply pressure,
τ : Squeeze terms,
– : Corresponding non-dimensional parameter,
* : Concentric operation.

Matrices

$\left[\overline{\mathbf{F}}\right]$: Fluidity matrix,
$\left[\overline{\mathbf{F}}_{\Gamma}\right]$: Global nodal force matrix,
$\{\overline{\mathbf{p}}\}$: Nodal pressure vector,
$\left\{\overline{\mathbf{Q}}\right\}$: Nodal flow vector,
$\left\{\overline{\mathbf{R}}_{\mathrm{H}}\right\}$: Column vector due to hydrodynamic terms,
$\left\{\overline{R}_{\mathrm{xj}}\right\}$, $\left\{\overline{R}_{\mathrm{zj}}\right\}$: Global right hand side vectors due to journal centre velocities.

Introduction

Hybrid journal bearings offer advantages of both the hydrostatic (high stiffness at low eccentricities, high accuracy of location and precision of rotation, cool operation. low wear) and hydrodynamic bearing (high load carrying capacity at high operating eccentricities) in one bearing.

In the hybrid mode of operation, the conventional multirecessed of pocketted journal bearings contribute very less towards hydrodynamic action [1–5]. The pockets of recesses constitute large bearing area in comparison to bearing lands. Therefore, the recessed journal bearing is not able to generate a substantial hydrodynamic pressure. Thus, recessed bearings when operating in hybrid mode at higher speeds are not suitable for heavily loaded applications. Therefore, to gain maximum advantages of both hydrostatic and hydrodynamic effects in a more efficient way, non-recessed i. e. hole-entry journal bearings are used for hybrid operations. The hole-entry journal bearings give better performance either as a hydrostatic bearing or as a hybrid bearing. In addition to this these are easy to manufacture and have reduced cost of machining.

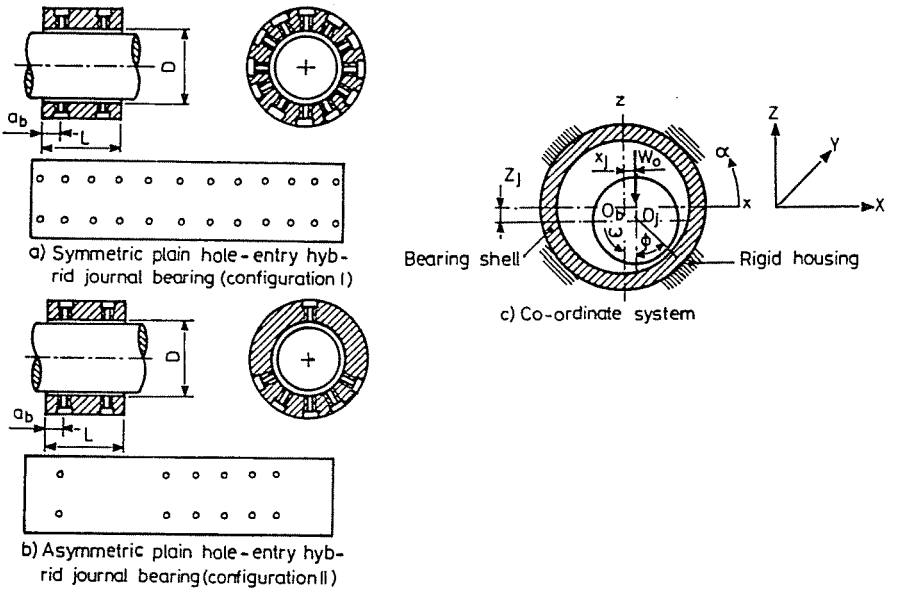

Fig. 1. Bearing geometry and co-ordinate system

In recent years, various theoretical and experimental studies have been carried out and reported in literature on non-recessed journal bearings [2–11]. These studies covered various aspects of these types of bearings, i. e., analysis, design, optimization, operation etc. The main observation regarding the available studies on hole-entry journal bearings is that these studies have been based on rigid bearing assumption i. e. both journal and bearing are assumed to be absolutely rigid. However, it is expected that when a bearing operates under heavy load, the pressure generated in the fluid film may be sufficient to cause significant deformation of bearing shell (of the order of fluid film thickness). The deformation in journal is ignored because the journal is generally made of harder material as compared to bearing shell. Thus, the flexibility of the bearing shell may affect the bearing performance characteristics.

The studies available on the elasto-hydrostatic analysis of hole-entry journal bearings are very limited. Recently various aspects of orifice-compensated multiple hole-entry journal bearing configuration [12] including bearing shell flexibility have been analyses. The study reveals that bearing shell flexibility should be considered in the analysis in order to establish design data more accurately.

The present work is an extension of the previous work [12] and is aimed at determining the effects of flexibility of bearing shell on the static

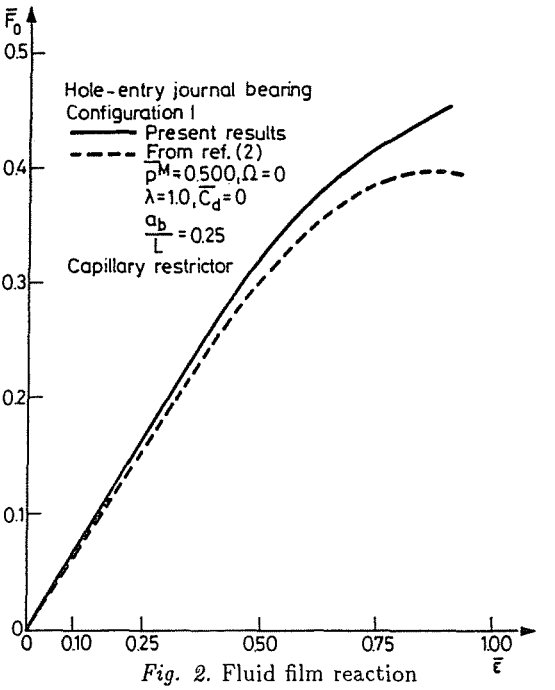

Fig. 2. Fluid film reaction

and dynamic performance characteristics of a constant flow valve compensated multiple hole-entry journal bearing configurations. Two hole-entry journal bearing configurations studied are the symmetrical hole-entry journal bearing with 12 holes per row and assymmetric hole-entry journal bearing with six holes per row [*Fig. 1*]. These configurations are referred as configurations I and configuration II respectively in the further discussion of this paper. Based on the normalization of the governing equations, a nondimensional parameter ($\overline{C}_d$) has been defined and can be regarded as a measure of the flexibility of bearing shell.

The bearing performance characteristics in terms of circumferential and axial pressure distributions, maximum or peak pressure ($\overline{p}_{\max}$), minimum film thickness ($\overline{h}_{\min}$), attitude angle (ϕ), stiffness coefficients ($\overline{S}_{11}$, $\overline{S}_{12}$, $\overline{S}_{21}$, $\overline{S}_{22}$), damping coefficients ($\overline{C}_{11}$, $\overline{C}_{12}$, $\overline{C}_{21}$, $\overline{C}_{22}$) and stability margin in terms of critical journal mass ($\overline{M}_c$), threshold speed ($\overline{\omega}_{\text{th}}$) and damped frequency of whirl ($\overline{\omega}_d$) have been presented for $\overline{C}_d = 0.0$, 0.1, 0.50, $\lambda = 1.0$, $\nu = 0.3$, $\Omega = 0.0$ and 1.00, $a_b/L = 0.25$. The input flows fed through each supply hole for configurations I and II are taken respectively as 0.12937 and 0.15514. These are the typical values of flow which corresponds to flow of lubricant through each supply hole for capillary

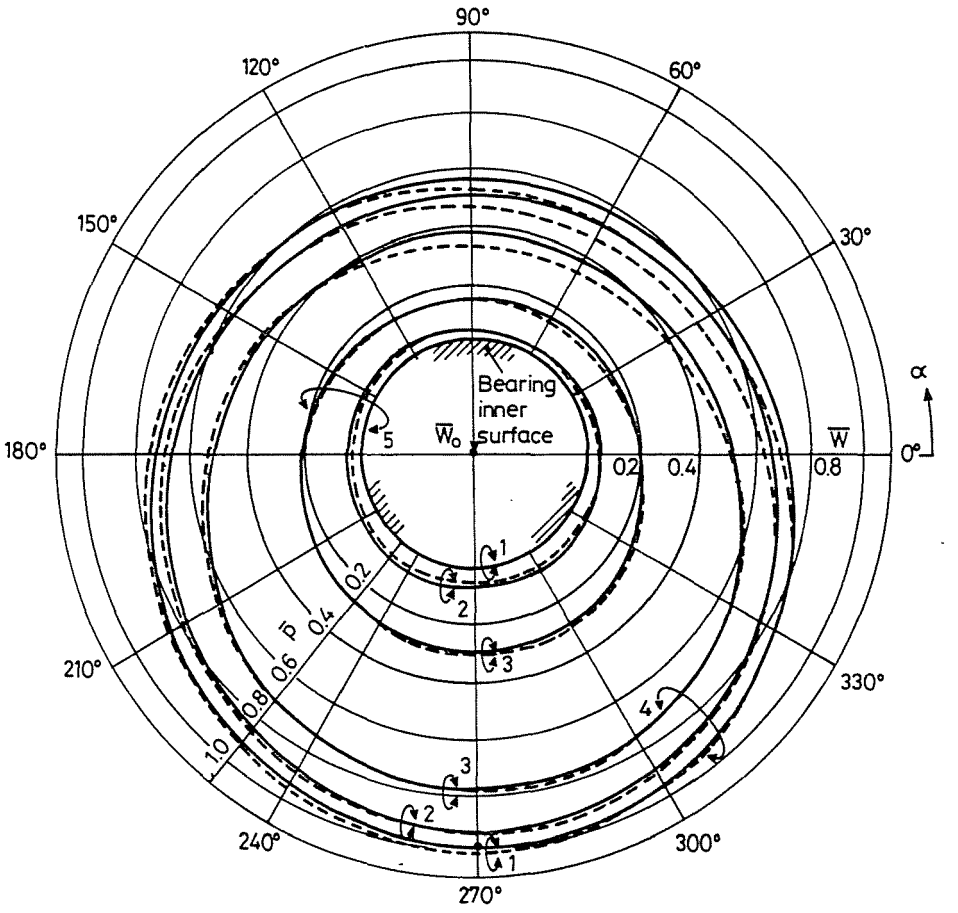

Configuration I	Curve No.	$\overline{C}_d$
——— $\Omega=0$	1	0
- - - - $\Omega=1.0$	2	0.1
Constant flow valve restrictor	3	0.5
$\overline{t}_h=0.1, \lambda=1.0, \overline{W}_o=1.0, \overline{Q}_n=0.12937$	4	pressure ($\overline{p}$)
Hole-entry journal bearing	5	deformation ($\overline{w}$)

Fig. 3. Circumferential pressure distribution and radial deformation at axial MID-plane

compensated rigid bearings, when operating concentrically and having a restricted design parameters ($\overline{C}_{s2}$) value equal to 0.5000. The ratio ($\overline{t}_h$) of bearing thickness (t_h) to journal radius (R_j) is taken as $\overline{t}_h=0.1$ [12].

Results presented in the paper will help in predicting the effects of bearing shell flexibility on the performance of constant flow valve compen-

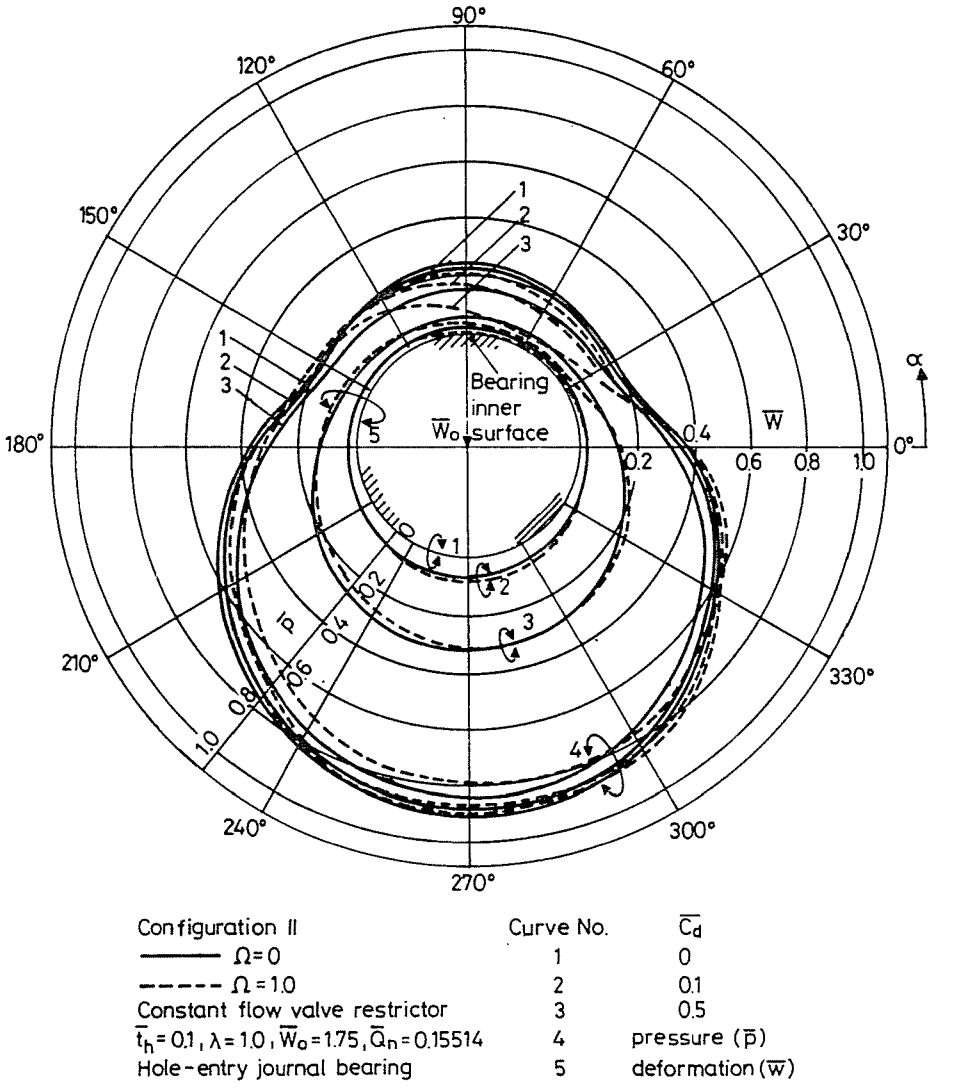

Fig. 4. Circumferential pressure distribution and radial deformation at axial MID-plane

sated multiple hole-entry journal bearings. The results will be useful to bearing designers.

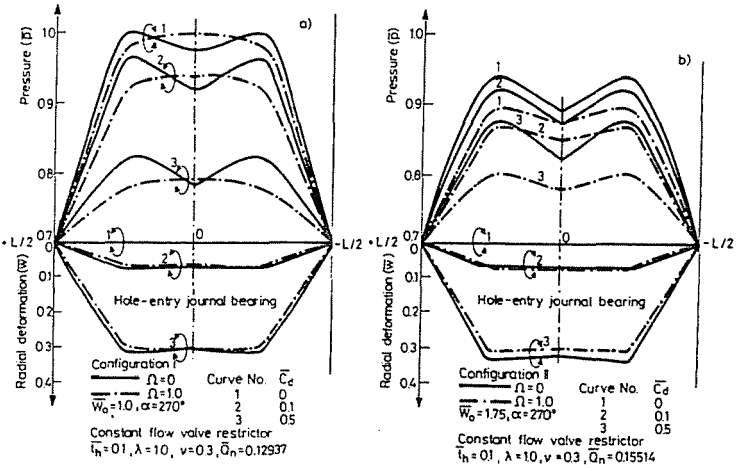

Fig. 5. a), b) Pressure distribution and radial deformation in axial direction

Analysis

Geometric details of the hole-entry journal bearing system are illustrated in *Fig. 1.* The laminar flow of isoviscous incompressible lubricant in the clearance space of a journal bearing system is governed by the following non-dimensional Reynolds equation.

$$\frac{\partial}{\partial\alpha}\left(\frac{\bar{h}^3}{12}\frac{\partial\bar{p}}{\partial\alpha}\right)+\frac{\partial}{\partial\beta}\left(\frac{\bar{h}^3}{12}\frac{\partial\bar{p}}{\partial\beta}\right)=\frac{1}{2}\Omega\frac{\partial\bar{h}}{\partial\alpha}+\frac{\partial\bar{h}}{\partial\tau}. \tag{1}$$

Using Galerkin's technique, the finite element method and equation (1), the system equation for the discretized flow field is derived [12] as:

$$\left[\overline{\mathbf{F}}\right]_{n_f x n_f}\left\{\overline{\mathbf{p}}\right\}_{n_f x_1}=\left\{\overline{\mathbf{Q}}\right\}_{n_f x_1}+\Omega\left\{\overline{\mathbf{R}}_H\right\}_{n_f x_1}+\overline{\dot{X}}_j\left\{\overline{\mathbf{R}}_{xj}\right\}_{n_f x_1}+\overline{\dot{Z}}_j\left\{\overline{\mathbf{R}}_{zj}\right\}_{n_f x_1} \tag{2}$$

where n_f is the total number of nodes in the lubricant flow field.

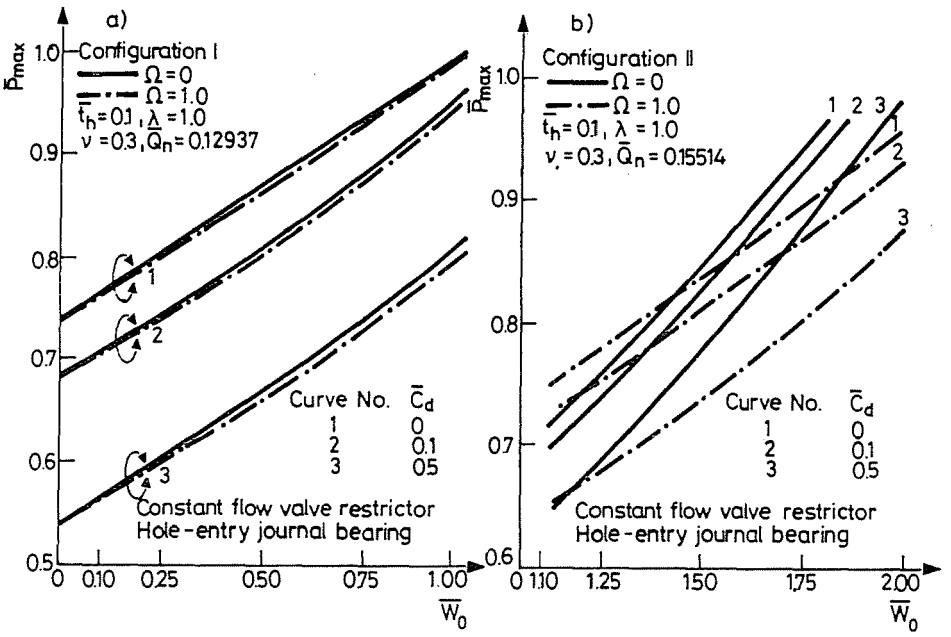

Fig. 6. a), b) Maximum pressure

Restrictor Flow Equation:

The flow ($\overline{Q}_R$) of lubricant through a constant flow valve restrictor is defined as

$$\overline{Q}_R = \text{Constant}\,,$$

$$Q_c = \overline{Q}_n\,. \tag{3}$$

An elastohydrostatic (EHS) analysis of a compensated hole-entry journal bearing system requires simulataneous solution of Reynolds equation, together with equations for the flow of lubricant through restrictors as constraint and three dimensional elasticity equations using appropriate boundary conditions for different solution domains and a suitable iterative scheme [12].

Results and Discussions

In the present study the size of supply holes are assumed to be quite small, and hence, the effects of pocket size have been neglected in computing the performance characteristics.

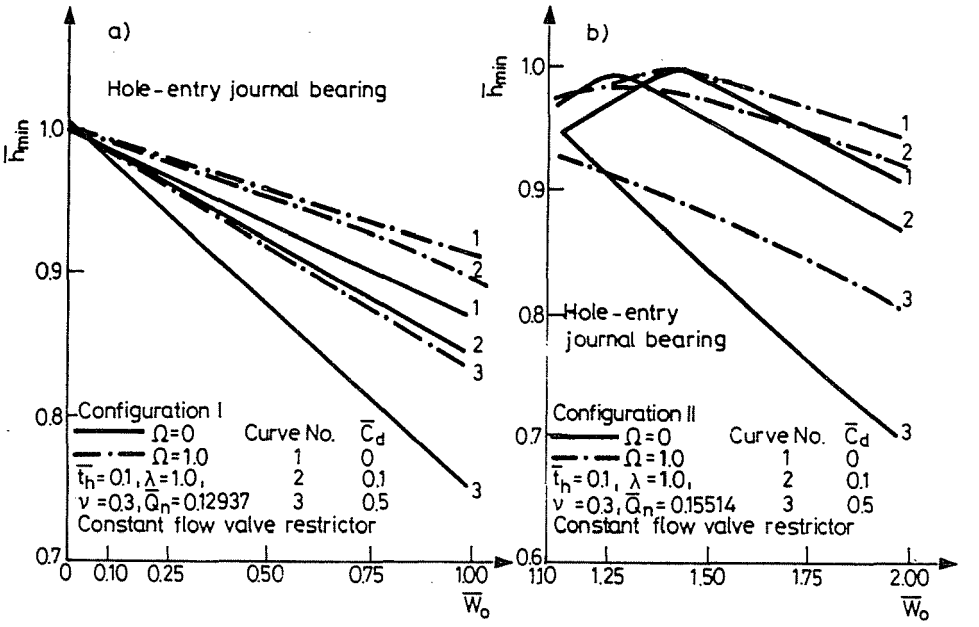

Fig. 7. a), b) Minimum film thickness

The performance characteristics of a constant flow valve compensated multiple hole-entry journal bearing system presented and discussed in this section were obtained using the analysis and computational technique decsribed in the previous section. The validity of the computer program used is tested by computing the validity of the computer program used is tested by computing the characteristics for a rigid bearing ($\overline{C}_d = 0.0$) and comparing these with the available results [2]. *Figure 2* shows a good agreement between the computed film reaction ($\overline{F}_o$) corresponding to different eccentricity ratios (ε) and those of [2] for capillary compensated bearing as the for constant flow valve compensated bearing are not available. Some differences between the computed and available results are seen at higher eccentricity ratios. This is probably due to the use of different computational techniques between the studies. The elastic deformation analysis program has been tested separately.

To study the effects of bearing shell flexibility, the bearing performance characteristics have been plotted against load ($\overline{W}_o$), for three representative of $\overline{C}_d$ (=0.0, 0.1, 0.5) [12]. With configuration II, it is possible to carry a load even at zero eccentricity ratio ($\varepsilon = 0.0$); the value of this load is $\overline{W}_o = 1.415$. Thus, the range of non-dimensional load $\overline{W}_o$ =1.0–2.0

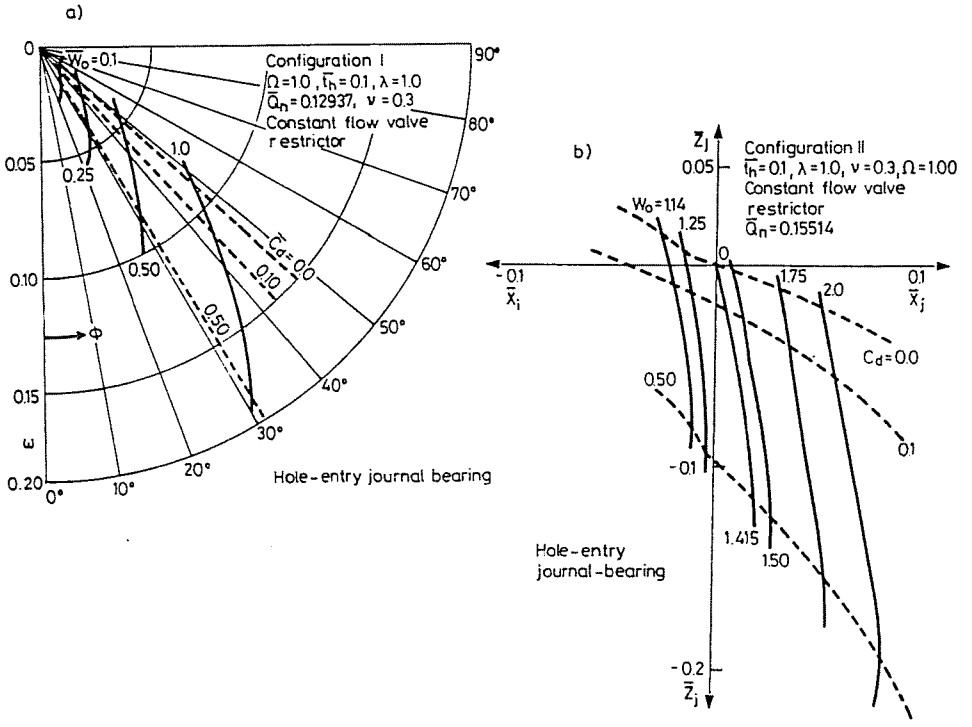

Fig. 8. a), Attitude angle *b*), Journal centre equilibrium position

is selected for the configuration II. Results for configuration I, have been obtained for the range of load $\overline{W}_o$=0.0–1.0. The range of non-dimensional load $\overline{W}_o$ =0.0–2.0 is selected so as to cover the generally used operating range of eccentricity.

The static performance characteristics have been presented in *Figs. 2–8. Figures 9–21* present the dynamic characteristics. At a fixed load ($\overline{W}_o$), the circumferential pressure distribution ($\overline{p}$) at the axial mid plane and the radial deformation ($\overline{w}$) for the hole-entry journal bearing configurations I and II have been shown in *Figs. 3* and *4*, both for hydrostatic as well as hybrid modes of operations.

In general, the fluid film pressure ($\overline{p}$) decreases with an increase in bearing shell flexibility ($\overline{C}_d$), both for hydrostatic as well as hybrid modes of operations and for both the configurations studied. *Fig. 5* shows the axial pressure distribution curves at an angular position α=270°. These curves

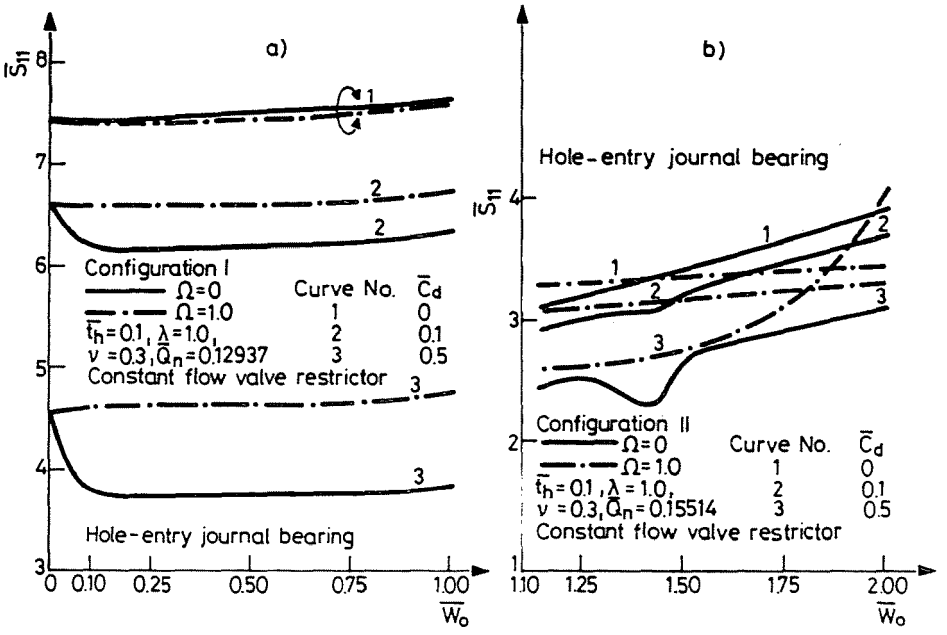

Fig. 9. a), b) Stiffness coefficient

depicts that radial deformation at any point increases with an increase in deformation coefficient ($\overline{C}_d$).

At a constant vertical load ($\overline{W}_o$), the maximum pressure ($\overline{p}_{max}$) (*Fig. 6*) is reduced as the bearing shell flexibility ($\overline{C}_d$) increases, for both hydrostatic as well as hybrid modes of operations. For a flexible bearing, the film thickness is a function of radial displacement ($\overline{w}$) of the fluid film — bearing shell — interface. An increased value of radial displacement ($\overline{w}$) and thus, the fluid film profile gets modified. This results in reduction in the value of $\overline{p}_{max}$.

Results of minimum film thickness ($\overline{h}_{min}$) have been presented in *Fig. 7*. A general of these results reveals the following:

1. In the case of configuration II, the constant flow valve compensated rigid journal bearing systems operates concentric ($\epsilon = 0.0$) when supporting an external load $\overline{W}_o = 1.415$ and therefore, $\overline{h}_{min}$ remains unity in this situation,
2. At constant load ($\overline{W}_o$), $\overline{h}_{min}$ value is reduced with an increase of bearing flexibility ($\overline{C}_d$) both for hydrostatic as well as hybrid modes

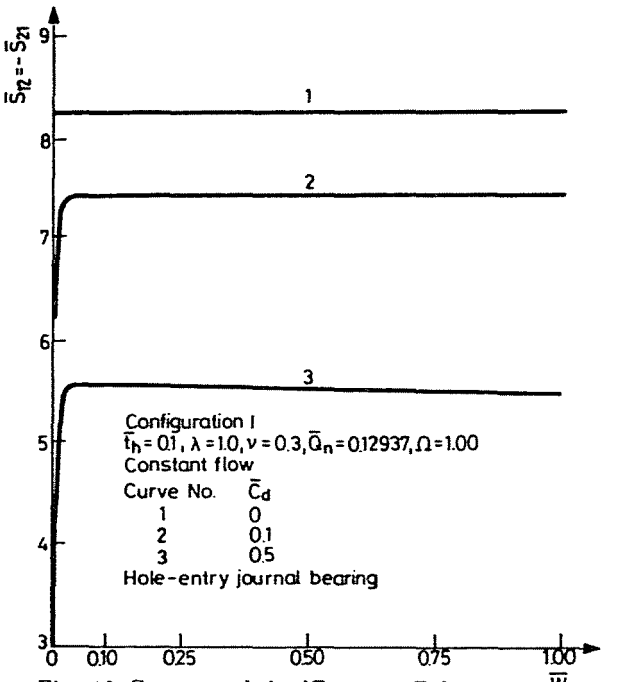

Fig. 10. Cross coupled stiffness coefficients

of operations as compared to the corresponding value for the rigid bearing case,

3. For flexible bearing, operating in hybrid mode of operation ($\Omega = 0.0$), the value of $\bar{h}_{\min}$ is generally more as compared to the corresponding values for the pure hydrostatic mode of operation,
4. At a constant load ($\bar{W}_o$), the reduction in the value of $\bar{h}_{\min}$ become more at large value of deformation coefficient (i. e. $\bar{C}_d = 0.500$).

Fig. 8 shows that so support a constant load, a flexible bearing system operates at higher eccentricity ratio (ε) and lower attitude angle (ϕ) than the corresponding rigid bearing system. This property is favourable from view point of dynamic performance.

The plots presented in *Figs. 9* through *12* shows the variations of fluid film stiffness coefficients. In the case of pure hydrostatic ($\Omega = 0.0$) mode of operation, the value of cross-coupled stiffness coefficients ($\bar{S}_{12}$, $\bar{S}_{21}$) obtained were zero. For the hybrid ($\Omega = 0.0$) mode of operation, the coupled stiffness coefficients were obtained to be equal in magnitude for configuration I. but not for configuration II. At a constant load ($\bar{W}_o$), the fluid film stiffness coefficients ($\bar{S}_{11}$, $\bar{S}_{12}$, $\bar{S}_{21}$, $\bar{S}_{22}$), decreases withy an

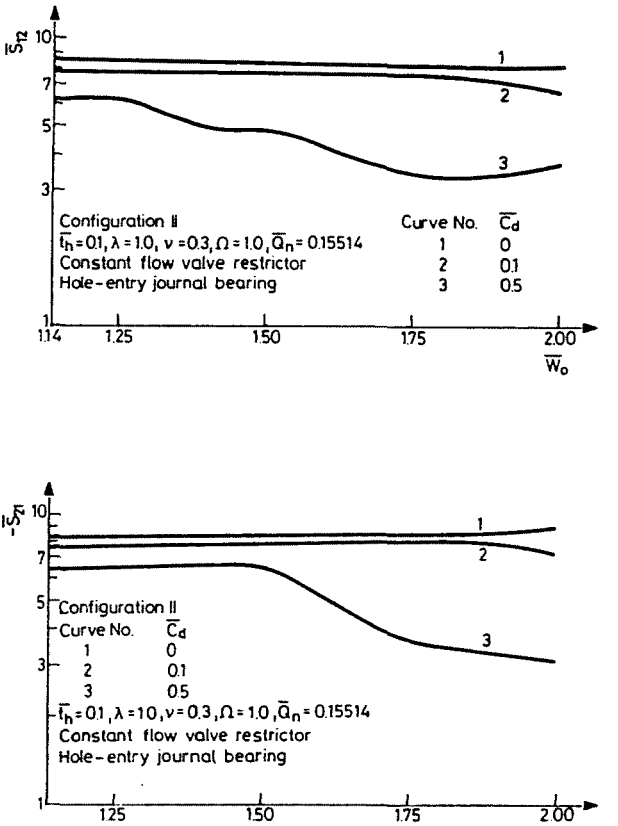

Fig. 11. Cross coupled stiffness coefficients

increase of bearing shell flexibility ($\bar{C}_d$), both for hydrostatic as well as hybrid modes of operation of bearings.

The effects of bearing shell flexibility ($\bar{C}_d$) on damping coefficients have been presented in *Figs. 13–15.* When the bearing operates in the hydrostatic mode ($\Omega = 0.0$) of operation, the coupled damping coefficients ($\bar{C}_{12}$, $\bar{C}_{21}$) are zero. Therefore, the variations in coupled damping coefficients are shown for hybrid mode of operation only, In general, at constant load ($\bar{W}_o$), the magnitude of damping coefficients ($\bar{C}_{11}$, $\bar{C}_{12}$, $\bar{C}21$, $\bar{C}_{22}$) decreases with an increase of bearing shell flexibility ($\bar{C}_d$), both for hydrostatic ($\Omega = 0.0$) as well as hybrid ($\Omega = 0.0$) modes of operational and for both the configurations studied.

The behaviour of coupled damping coefficients ($\bar{C}_{12}$, $\bar{C}_{21}$), for configuration II, is opposite in nature if the load is greater or less than the load carrying capacity of the rigid bearing at zero eccentricity ratio ($\varepsilon = 0.0$)

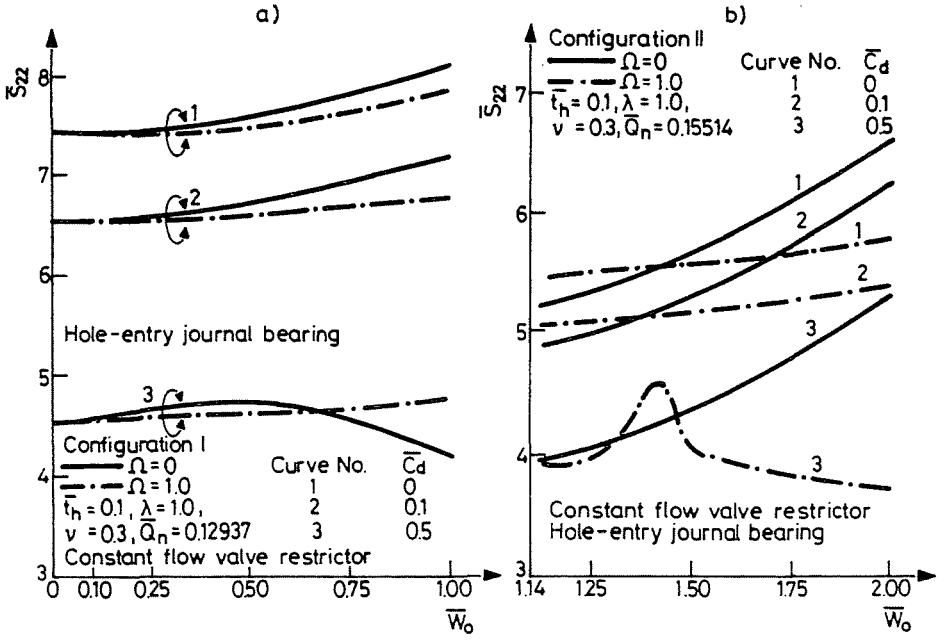

Fig. 12. a), b) Stiffness coefficient

i. e. $\overline{W}_o = 1.415$. the coupled damping coefficients have identical valves for both the configurations studied. For configuration I, the coupled damping coefficients are very small in comparison to direct damping coefficient and remains negative over the entire load range.

Figs. 16 through *21*, shows the variations of the stability margin parameters $\overline{M}_c$, $\overline{\omega}_{th}$ and $\overline{\omega}_d$ due to bearing shell flexibility. The variations in the stability margin parameters have been presented only for hybrid mode of operation. When the flexible bearing operates in the pure hydrostatic ($\Omega = 0.0$) mode, then owing to the absence of cross-coupled stiffness and damping coefficients terms, the stability margin parameters ($\overline{M}_c$, $\overline{\omega}_{th}$, $\overline{\omega}_d$) of the journal bearing system assumes values such that the system remains always stable.

At a constant load ($\overline{W}_o$), the values of $\overline{M}_c$ and $\overline{\omega}_{th}$ decreases with an increase of $\overline{C}_d$ for Configuration I, *Figs. 16* and *18*. While for configuration II, the behaviour of plots of $\overline{M}_c$ and $\overline{\omega}_{th}$ due to increase in bearing shell flexibility ($\overline{C}_d$) id opposite in nature for load below and above the load $\overline{W}_o = 1.415$, *Figs. 17* and *19*.

The damped frequency of whirl ($\overline{\omega}_d$) for the hole-entry journal bearing configuration I, *Fig. 20*, gets stabilized between values 0.40 and 0.50 for

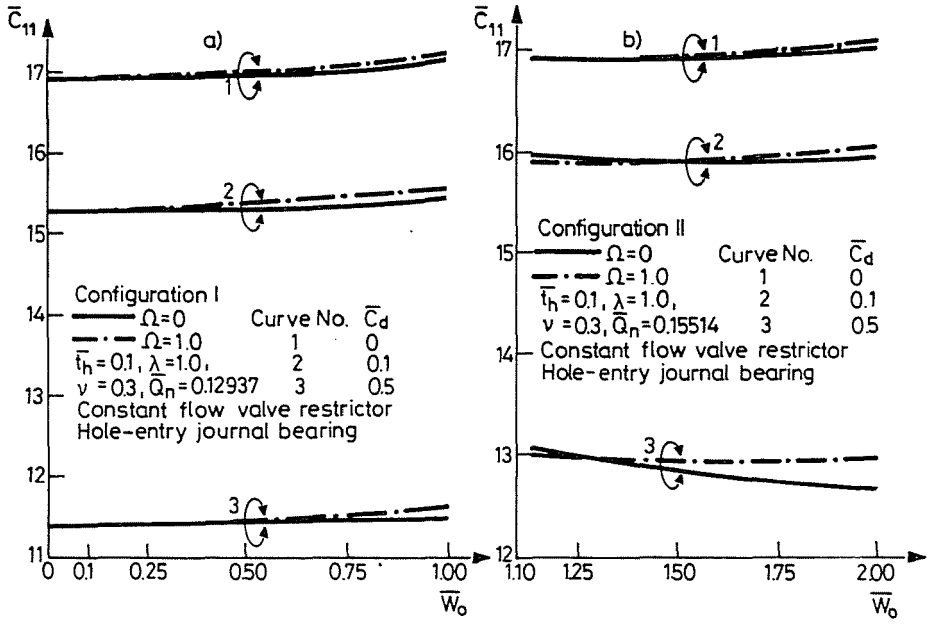

Fig. 13. a), b) Damping coefficient

loads ($\overline{W}_o$ =0.1–1.0) when $\overline{C}_d$ is increased. However, for configuration II, $\overline{\omega}_d$ increases with the increase of bearing shell flexibility ($\overline{C}_d$), *Fig. 21.*

Numerical Example

A numerical example is provided to illustrate the effects of bearing shell flexibility on bearing performance characteristics.

A hole-entry journal bearing with 12 holes per row, configuration I, *Fig. 1,* using constant flow valve compensation has been analyzed for the following geometric and operating data:

R_j	= 50 mm,	$\frac{a_b}{L}$	= 0.25,
t_{th}	= 5mm,	$\overline{p}^*$	= 0.5000,
λ	= 1.0,	μ	= 0.0345 N· s· m^{-2} at 38°C,
ϱ	= 858 kg·m^{-3},	c	= 0.05020 mm,
N	= 2500 rpm,	p_s	= 8.96 MN/m^2,
Ω	= 1.0,	W_o	= 22.4 kN,
		$\overline{W}_o$	= 1.00.

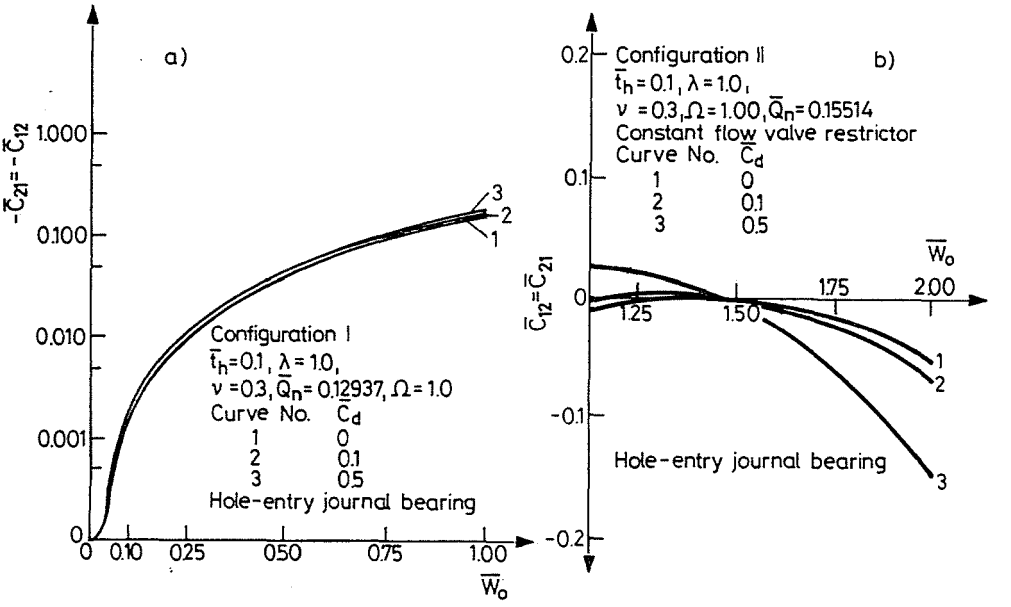

Fig. 14. Cross coupled damping coefficient

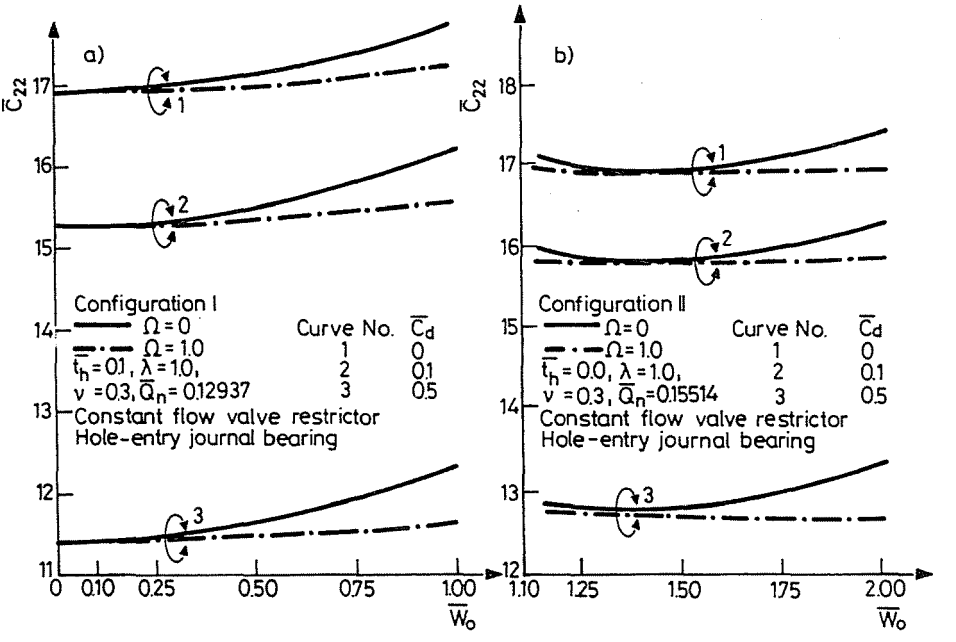

Fig. 15. a), b) Damping coefficient

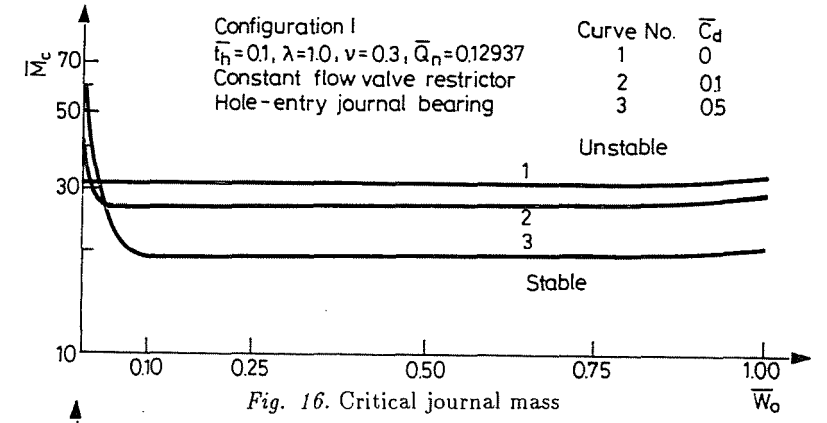

Fig. 16. Critical journal mass

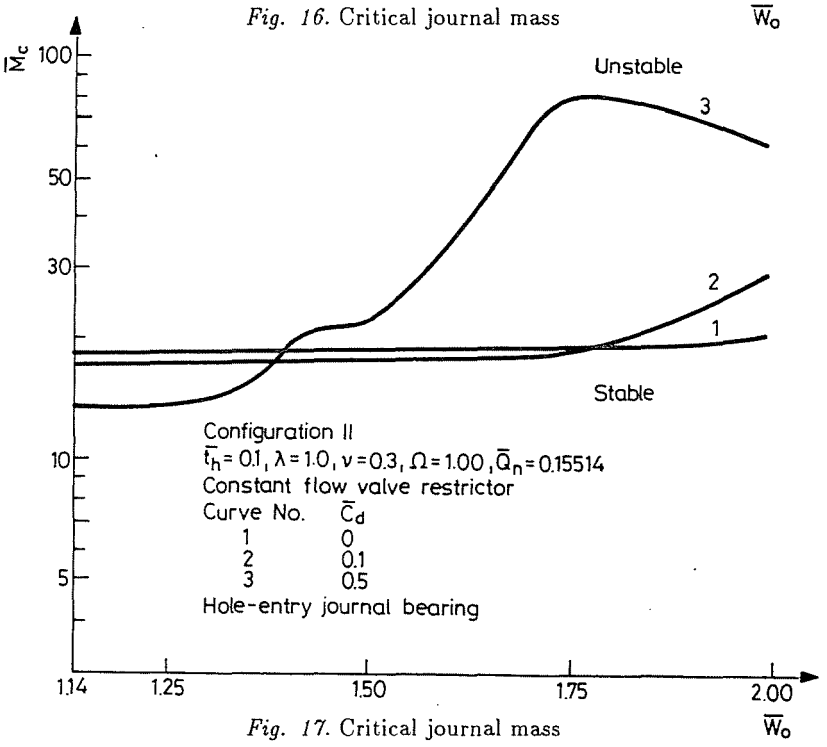

Fig. 17. Critical journal mass

The dimensional values of performance characteristics of a hole-entry hybrid flexible journal bearing, configuration I are presented in *Table 1.*

The percentage changes in the values of bearing performance characteristics for a flexible bearing system as shown in *Table 2,* have been computed with respect to the corresponding values for rigid bearing cases.

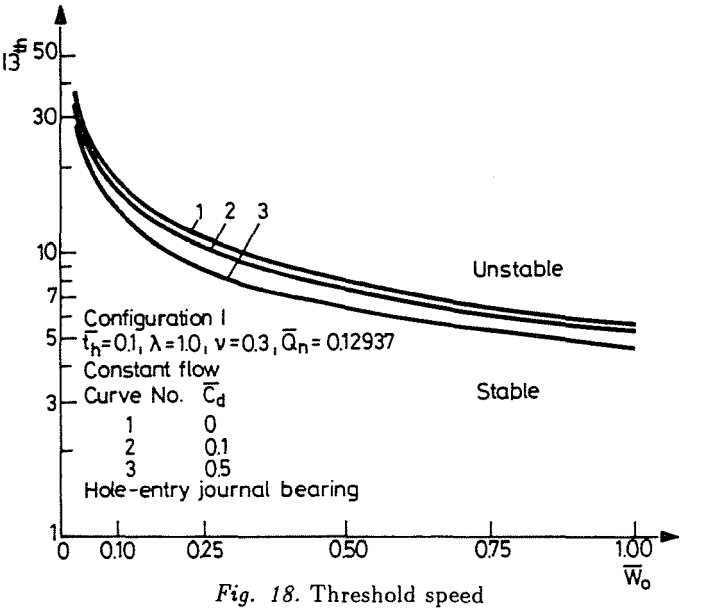

Fig. 18. Threshold speed

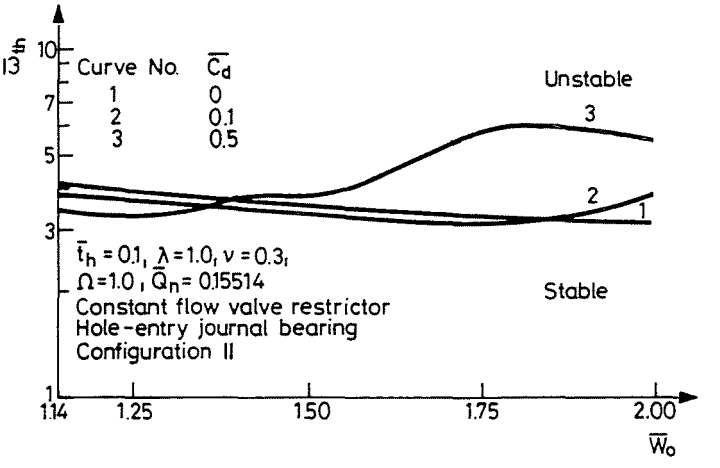

Fig. 19. Threshold speed

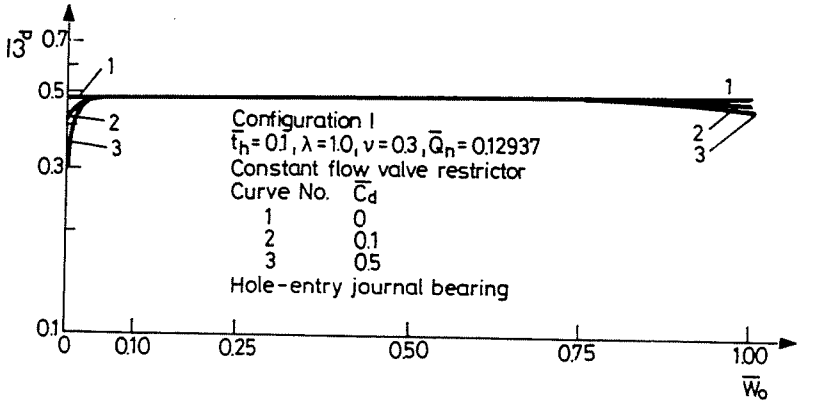

Fig. 20. Frequency of whirl

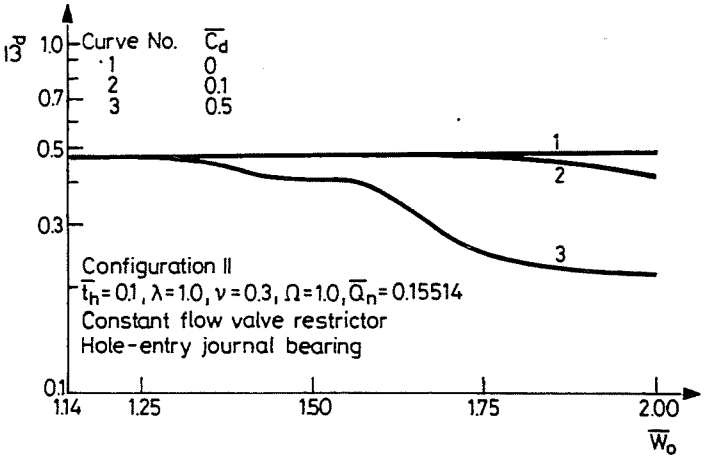

Fig. 21. Frequency of whirl

Table 1
Performance characteristics of hole-entry hybrid journal bearing with constant valve compensation
CONFIGURATION I

Specimen No.	1	2	3	4	5	6
Performance Characteristics $\overline{C}_d$	0.000	0.004462	0.170252	0.0308073	0.1406505	0.3982281
ν	—	0.303	0.357	0.44	0.40	0.47
p_{max} Nmm^2	0.76527	0.76375	0.76045	0.76049	0.73586	0.73190
h_{min} mm	0.89762	0.89715	0.89615	0.89637	0.88841	0.8900
$\phi_{(deg.)}$	59.14721	58.83813	58.17677	58.20680	53.38637	52.88394
S_{11} MN/mm	5.1453	5.1265	5.0858	5.0864	4.7863	4.7421
S_{12} MN/mm	8.2998	8.2706	8.2078	8.2095	7.7453	7.6850
$-S_{21}$ MN/mm	−8.5099	−8.4821	−8.4221	−8.4239	−7.9782	−7.9202
S_{22} MN/mm	5.1881	5.1681	5.1241	5.1249	4.7996	4.7509
C_{11} MNs/mm	17.3979	17.3291	17.2027	17.2063	16.2686	16.1480
$C_{12}=C_{21}$ MNs/mm	−0.1941	−0.1943	−0.1946	−0.1945	−0.1972	−0.1965
C_{22} MNs/mm	17.1834	17.1258	17.0017	17.0050	16.0853	15.9642
M_c 10^6·kg	36.881	36.744	36.446	36.451	34.2466	33.918
ω_{th} rad/s	2066.321	2062.475	2054.075	2054.208	1991 .038	1981.622
ω_d rad/s	214.942	214.933	214.925	214.925	214.827	214.814

$\overline{p}=0.5000$; $p_s=8.96$ N·mm; $\overline{W}_o=1.0$ $W_o=22.4$ kN; $\Omega=1.00$; $N=2500$ rpm.

Table 2

Percentage change in performance characteristics of hole-entry hybrid journal bearing with constant flow valve compensation

Specimen No.		1	2	3	4	5	6
Performance Characteristics	$\overline{C}_d$	0.000	0.004462	0.170252	0.030807	0.1406505	0.3982281
	ν	—	0.303	0.357	0.44	0.40	0.47
p_{max}		—	−0.1986	−0.6298	−0.6246	−3.843	−4.3605
h_{min}		—	−0.0524	−0.1637	−0.1392	−1.0261	−0.8489
$\phi_{(deg.)}$		—	−0.5225	−1.6407	−1.5899	−9.7390	−10.5899
S_{11}		—	−0.3208	−1.1122	−1.1005	−6.9356	−7.7951
S_{12}		—	−0.3518	−1.1085	−1.0879	−6.6808	−7.4074
$-S_{21}$		—	−0.3266	−1.0374	−1.01059	−6.2480	−6.9296
S_{22}		—	−0.3855	−1.2336	−1.2182	−7.4883	−8.4269
C_{11}		—	−0.3382	−1.0651	−1.0444	−6.4372	−7.1308
$C_{12}=C_{21}$		—	0.1030	0.2579	0.2061	1.5971	1.2364
C_{22}		—	−0.3352	−1.0574	−1.0382	−6.3905	−7.0952
M_c		—	−0.37026	−1.1794	−1.1666	−7.1439	−8.0327
ω_{th}		—	−0.18612	−0.5926	0.5861	−3.643	−4.0990
ω_d		—	−0.004113	−0.00822	−0.008226	−0.008226	−0.05964

$\overline{p}=0.5000$; $p_s=8.96\,\text{N}\cdot\text{mm}$; $\overline{W}_o=1.0$; $W_o=22.4\,\text{kN}$; $\Omega=1.00$; $N=2500\,\text{rpm}$.

$$\%\ change\ in\ P.C. = \frac{(P.C.)_{flexible}-(P.C.)_{rigid}}{(P.C.)_{rigid}} \cdot 100$$

$P.C. = performance\ characteristics$

Conclusions

Based on the results presented in previous sections, if a constant vertical load is to be supported, the following observations apply:

. In general, the values of bearing performance characteristics such as maximum pressure ($\overline{p}_{max}$), attitude angle (ϕ), stiffness coefficients and damping coefficients decreases with the increase of bearing shell flexibility ($\overline{C}_d$), when the bearing operate in hydrostatic– hybrid mode of operation.

. The value of minimum film thickness ($\overline{h}_{min}$) is reduced with the increase in $\overline{C}_d$ and/or load ($\overline{W}_o$). A flexible hole–entry journal bearing system is superior from the view point of $\overline{h}_{min}$, when operating in hybrid mode of operation.

. An increase in bearing shell flexibility ($\overline{C}_d$) improves the stability margin ($\overline{M}_c$, $\overline{\omega}_{th}$) of hole–entry journal bearing configuration II at higher loads, while for configuration I, the stability margin decreases. These results, therefore suggests the need for a careful disposition of supply holes around the circumference of a bearing geometry.

. The elastohydrostatic effects in the study of hole–entry journal bearings are significant when load is heavy and/or deformation coefficient ($\overline{C}_d$) is large. In the numerical example a reduction of 8.43% is noticed in the value of stiffness coefficient ($\overline{S}_{22}$).

References

1. ROWE, W. B (1983): Hydrostatic and Hybrid Bearing Design, Butterworths, London.
2. ROWE, W. B. – XU, S. X. – CHONG, F. S. – WESTON, W.: *Tribology Int.* Vol. 15, pp. 339–348 (1982).
3. STOUT, K. J. – ROWE, W. B.: *Tribology Int.* Vol. 7, pp. 195–212 (1974).
4. STOUT, K. J. – ROWE, W. B.: *Tribology Int.* Vol. 7, pp. 98–106 (1974).
5. ROWE, W. B. – KOSHAL, D. – STOUT, K. J.: *Jour. of Mech. Eng. Science,* Vol. 18, pp. 73– 78 (1976).
6. ROWE, W. B. – KOSHAL, D., (1980): *Wear.* Vol. 64, pp. 115–131.
7. KOSHAL, D. – ROWE, W. B., (1981): *Trans, ASME.* Vol. 103, pp. 558–565.
8. KOSHAL, D. – ROWE, W. B. (1981): *Trans, ASME.* Vol. 103, pp. 566–572.
9. EL KAYAR, A. – SALEM, E. A. – KHALIL, M. F. – HEGAZY, A. A. (1983): *Wear.* Vol. 54, pp. 1–13.
10. IVES, J. – ROWE, W. B.: The Effect of Multiple Supply Sources on the Performance of Heavily Loaded Pressurized High Speed Journal Bearing's *Proc. Int. Conf. Tribology, Inst. Mech. Engrs.* paper C199/87.
11. YOSHIMOTO, S. – ROWE, W. B. – IVES, J.: *Wear.* Vol. 127, pp. 307–318 (1988).
12. SHARMA, S. C. – SINHASAN, R. – JAIN, S. C.: *Int. J. Mach. Tool Manufact.* Vol. 30, pp. 111–129 (1990).

Address: S. C. SHARMA, S. C. JAIN, R. SINHASAN
Department of Mechanical and Industrial Engineering
University of Roorkee, India 247667